J. Fluid Mech. (1988), *vol.* 195, *pp.* 413–435
Printed in Great Britain

Unsteady laminar boundary layer along the symmetry plane of an impulsively started prolate spheroid

By W. C. XU AND K. C. WANG
Aerospace Engineering and Mechanics, San Diego State University, San Diego, CA 92182, USA

(Received 24 June 1987 and in revised form 26 February 1988)

The symmetry-plane laminar boundary layer over an impulsively-started prolate spheroid of axes ratio 1/4 at various incidence is calculated in detail. Results agree with the steady solutions at large times. The most important one is concerned with the similarity between the distribution of the leeside skin friction at a fixed incidence, but varying in time, and that of the leeside skin friction for steady flows varying in incidence. The latter patterns led previously to the concept of an open and closed separation sequence for steady flows, likewise the newly found similarity suggests an unsteady open and closed sequence; i.e. at low incidence, separation starts around the rear stagnation point and gradually expands upstream in time, but it is always of the closed type. At moderate to high incidence, closed separation prevails at small times, open separation develops at large times, but separation may either remain open at moderate incidence or return to closed at high incidence as the steady-state condition is approached. The rate of approach toward the steady-state condition increases with incidence. For a less slender spheroid there is no open separation involved; unsteady separation lines are all of the closed type. For bodies other than spheroids, similar ideas may be applied.

1. Introduction

The present work considers the unsteady laminar boundary layer along the symmetry-plane of an impulsively-started prolate spheroid of which the axes ratio b/a is 1/4 (figure 1). This is undertaken as a prelude to full three-dimensional investigations over the entire body. Once the flow behaviour along both the windside and the leeside symmetry planes is well understood, a great deal can be learned regarding the overall flow on the whole body. Complete solutions of genuine unsteady three-dimensional boundary layers still remain scarce at present.

The same problem was first initiated by Wang & Fan (1982), but calculations then were confined to the nose region at a single incidence (45°). As restrictive as they were, some conclusions from this previous work have been confirmed by the present more detailed calculations.

In this work, calculations were made along the entire symmetry-plane of the prolate spheroid at incidence 6°, 30°, 45° and 50°. Both windside and leeside were included, except in the 6° incidence case where only the leeside was calculated because the windside problem at such a low incidence was thought to deviate very little from the axisymmetric case, and hence not many new features could be expected.

The relevant governing equations are presented in §2; brief descriptions of the

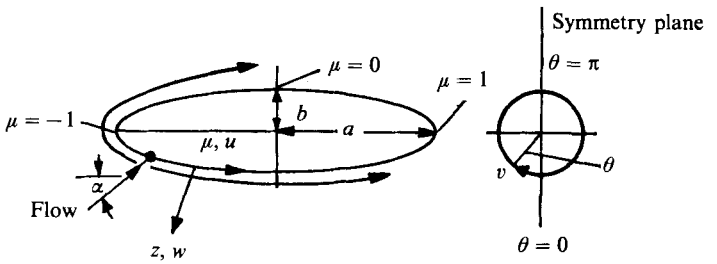

FIGURE 1. Prolate spheroid ($b/a = 1/4$), coordinates and notations.

method of solution in §3 and results in §4. Among the most interesting features obtained is the similarity between the distribution of the unsteady leeside skin friction varying in time, but at a fixed incidence, and the distribution of the steady leeside skin friction varying in incidence. The latter distribution was used previously as the basis in developing the idea of the open and closed separation sequence in steady flows (Wang 1972). This idea, first conceived according to the symmetry-plane studies (Wang 1970), was later confirmed by full three-dimensional calculations and by experiments. Based on the similarity just mentioned, an unsteady open and closed separation sequence is proposed using similar arguments. Preliminary aspects of this unsteady open and closed sequence have been presented before (Wang & Fan 1982), but a more complete picture, as presented in §5, has only been reached as a result of the present more detailed calculations. This proposed sequence is fundamentally different from the conventional notion of unsteady three-dimensional separations. More details of the present work have been previously reported (Xu & Wang 1987).

2. Equations

The governing equations for the present symmetry-plane boundary layer written in non-dimensional form are

$$\frac{\partial u}{\partial t}+u\frac{\partial u}{h_\mu \partial \mu}+w\frac{\partial u}{\partial z}=\frac{-\partial p}{h_\mu \partial \mu}+\frac{\partial^2 u}{\partial z^2}, \tag{1a}$$

$$\frac{\partial v_\theta}{\partial t}+u\frac{\partial v_\theta}{h_\mu \partial \mu}+w\frac{\partial v_\theta}{\partial z}+\frac{v_\theta^2}{r}+\frac{uv_\theta}{r}\frac{\partial r}{h_\mu \partial \mu}=-\frac{\partial^2 p}{r\,\partial \theta^2}+\frac{\partial^2 v_\theta}{\partial z^2}, \tag{1b}$$

$$\frac{\partial u}{h_\mu \partial \mu}+u\frac{\partial r}{r h_\mu \partial \mu}+\frac{v_\theta}{r}+\frac{\partial w}{\partial z}=0. \tag{1c}$$

Briefly, referring to figure 1, α is the incidence angle, μ and θ are two surface coordinates and z is the normal coordinate. The corresponding velocities are u, v and w, and U and V are the inviscid velocities at the outer edge. The metric coefficients are h_μ and r; and r, in fact, is also the cross-sectional radius.

$$h_\mu = [(1-e^2\mu^2)/(1-\mu^2)]^{\frac{1}{2}},$$

$$r = [(1-e^2)(1-\mu^2)]^{\frac{1}{2}},$$

where

$$e = (1-b^2/a^2)^{\frac{1}{2}},$$

a and b are the semi-major and -minor axis of the ellipsoid.

At the plane of symmetry, $v = 0$, so that $v_\theta (= \partial v/\partial\theta)$ is taken as an independent variable along with u and w. The boundary conditions are

$$u = U, \quad v_\theta = V_\theta \quad (\text{i.e. } \partial V/\partial\theta) \quad \text{at } z \to \infty, \tag{2a}$$

$$U = v_\theta = 0 \quad \text{at } z = 0, \tag{2b}$$

where U, V_θ and the pressure gradients are known;

$$U = \frac{1}{(1-e^2\mu^2)^{\frac{1}{2}}}[(1+k_a)(\cos\alpha)(1-\mu^2)^{\frac{1}{2}} + (b/a)(1+k_c)(\sin\alpha)\mu\cos\theta], \tag{3a}$$

$$V_\theta = (1+k_c)\sin\alpha\cos\theta, \tag{3b}$$

$$-\frac{\partial p}{h_\mu \partial\mu} = \frac{(1+k_a)^2\cos^2\alpha}{(1-e^2\mu^2)^{\frac{1}{2}}}[(1-\mu^2)^{\frac{1}{2}} + \lambda\mu\cos\theta]\left\{-\mu + \lambda(\cos\theta)(1-\mu^2)^{\frac{1}{2}} + \frac{e^2\mu}{1-e^2\mu^2}[1-\mu^2+\lambda\mu\cos\theta(1-\mu^2)^{\frac{1}{2}}]\right\}, \tag{3c}$$

$$-\frac{\partial^2 p}{\partial\theta^2} = \frac{1}{(b/a)}(1+k_a)(1+k_c)\cos\alpha\sin\alpha\left\{\lambda - \left(\frac{b}{a}\right)^2 \frac{\mu\cos\theta}{1-e^2\mu^2}[(1-\mu^2)+\lambda\mu\cos\theta]\right\}, \tag{3d}$$

with

$$\lambda = \left(\frac{b}{a}\right)\frac{(1+k_c)\sin\alpha}{(1+k_a)\cos\alpha},$$

$$k_a = \left[\frac{1}{2e}\log\frac{1+e}{1-e} - 1\right] \Big/ \left[\frac{1}{1-e^2} - \frac{1}{2e}\log\frac{1+e}{1-e}\right], \quad k_c = \frac{1}{1+2k_a}.$$

Based on the u-velocity, the skin friction and the displacement thickness are defined by

$$c_{f\mu} = \frac{1}{R^{\frac{1}{2}}}\left(\frac{\partial u}{\partial z}\right)_{z=0}, \tag{4a}$$

$$\Delta^*_\mu = \int_0^\infty (1-u/U)\,\mathrm{d}z. \tag{4b}$$

Analogously, we define based on the v_θ-profile,

$$(c_f)_{v\theta} = \frac{1}{R^{\frac{1}{2}}}\left(\frac{\partial v_\theta}{\partial z}\right)_{z=0}, \tag{4c}$$

$$\Delta^*_{v\theta} = \int_0^\infty (1-v_\theta/V_\theta)\,\mathrm{d}z. \tag{4d}$$

In applying the equation for unsteady total displacement thickness (Moore & Ostrach 1957)

$$\nabla\cdot\left[\rho_1 q_1 \Delta^* - \int_0^\infty (\rho_1 q_1 - \rho q)\,\mathrm{d}z\right] + \frac{\partial}{\partial t}\left[\rho_1\Delta^* - \int_0^\infty (\rho_1-\rho)\,\mathrm{d}z\right] = 0, \tag{5a}$$

to the symmetry-plane case, care must be taken to incorporate $\Delta^*_{v\theta}$ into the final expression

$$\frac{\partial\Delta^*}{\partial t} + \frac{1}{rh_\mu}\frac{\partial}{\partial\mu}[rU(\Delta^* - \Delta^*_\mu)] + \frac{V_\theta}{r}(\Delta^* - \Delta^*_{v\theta}) = 0, \tag{5b}$$

where Δ^* is the total displacement thickness, q is the resultant velocity and subscript 1 refers to the outer edge of the boundary layer. In this work, only Δ^*_μ is presented, Δ^* was not calculated.

For two-dimensional unsteady problems, Wang (1979) defined analogous limiting streamlines in the (x, t)-plane (or (μ, t)-plane in the present case) by

$$\left.\begin{aligned} \frac{h_\mu \mathrm{d}\mu}{\mathrm{d}t}\bigg|_{z=0} &= \boldsymbol{u}_{z=0} + \left(\frac{\partial \boldsymbol{u}}{\partial z}\right)_{z=0} \Delta z + \ldots \\ &= c_{f\mu} R^{\frac{1}{2}} \Delta z + \ldots, \end{aligned}\right\} \tag{6}$$

where $R^{\frac{1}{2}}\Delta z$ may be considered as a scale factor because it does not change the overall flow pattern. The unsteady separation is then identified by the running-together of those limiting streamlines. The same method is used in the present symmetry-plane problem.

3. Method of solution

Equations (1*a–c*) are similar in structure to those for three-dimensional steady boundary layers investigated before (Wang 1974), therefore the same numerical methods and computer programs developed earlier were used here.

3.1. *Initial profiles*

To start the computations, two sets of initial profiles, temporal and spatial, are required.

Immediately after the start, potential flow prevails. The usual first approximation of a small-time expansion may be used as the temporal initial profiles ($t = t_0$),

$$U(t_0, \mu, z) = U(\mu)\,\mathrm{erf}\left(\frac{z}{2t_0}\right), \tag{7a}$$

$$V_\theta(t_0, \mu, z) = V_\theta\,\mathrm{erf}\left(\frac{z}{2t_0}\right). \tag{7b}$$

where erf is the error function.

Based on the argument that diffusion and convection within the framework of boundary-layer theory affect the downstream flow only, solutions near the front stagnation point may be considered to be nearly independent of time. Thus, the required spatial initial profiles are provided by the steady symmetry-plane solution near the stagnation point.

3.2. *Difference schemes*

A Crank–Nicolson type of the finite difference method (Wang 1979) was used. In regions where no reversal of the u-velocity occurs:

$$\left(\frac{\partial(\,)}{\partial t}\right)_{l+\frac{1}{2}, m+\frac{1}{2}, n} = \frac{(\,)_{l+1, m+1, n} - (\,)_{l, m+1, n} + (\,)_{l+1, m, n} - (\,)_{l, m, n}}{2\Delta t}, \tag{8a}$$

$$\left(\frac{\partial(\,)}{h_\mu \partial\mu}\right)_{l+\frac{1}{2}, m+\frac{1}{2}, n} = \frac{1}{2}\left[\frac{(\,)_{l+1, m+1, n} - (\,)_{l+1, m, n}}{(h_\mu)_{m+\frac{1}{2}}\Delta\mu} + \frac{(\,)_{l, m+1, n} - (\,)_{l, m, n}}{(h_\mu)_{m+\frac{1}{2}}\Delta\mu}\right], \tag{8b}$$

$$\left(\frac{\partial(\ )}{\partial z}\right)_{l+\frac{1}{2},m+\frac{1}{2},n} = \frac{1}{2}\left[\frac{(\ )_{l+1,m+1,n}-(\ )_{l+1,m+1,n-1}}{2\Delta z}+\frac{(\ )_{l,m+1,n}-(\ )_{l,m,n-1}}{2\Delta z}\right], \tag{8c}$$

$$\left(\frac{\partial^2(\ )}{\partial z^2}\right)_{l+\frac{1}{2},m+\frac{1}{2},n} = \frac{1}{2(\Delta z)^2}[(\ )_{l+1,m+1,n+1}-2(\ )_{l+1,m+1,n}+(\ )_{l+1,m+1,n-1} + (\ )_{l,m,n+1}-2(\ )_{l,m,n}+(\ )_{l,m,n-1}]. \tag{8d}$$

But in regions where reversal of the u-velocity does occur, a zig-zag scheme (Krause 1969; Wang 1979) is used in order to satisfy the dependence rule (Wang 1975),

$$\left(\frac{\partial(\ )}{\partial t}\right)_{l-\frac{1}{2},m,n} = \frac{(\ )_{l+1,m,n}-(\ )_{l,m,n}}{2\Delta t}, \tag{9a}$$

$$\left(\frac{\partial(\ )}{h_\mu \partial\mu}\right)_{l-\frac{1}{2},m,n} = \frac{1}{2}\left[\frac{(\ )_{l+1,m,n}-(\ )_{l+1,m-1,n}}{(h_\mu)_{m-\frac{1}{2}}\Delta\mu}+\frac{(\ )_{l,m+1,n}-(\ )_{l,m,n}}{(h_\mu)_{m+\frac{1}{2}}\Delta\mu}\right], \tag{9b}$$

$$\left(\frac{\partial(\ )}{\partial z}\right)_{l+\frac{1}{2},m,n} = \frac{1}{2}\left[\frac{(\ )_{l+1,m,n+1}-(\ )_{l+1,m,n-1}}{2\Delta z}+\frac{(\ )_{l,m,n+1}-(\ )_{l,m,n-1}}{2\Delta z}\right], \tag{9c}$$

$$\left(\frac{\partial^2(\ )}{\partial z^2}\right)_{l+\frac{1}{2},m,n} = \frac{1}{2(\Delta z)^2}[(\ )_{l+1,m,n+1}-2(\ )_{l+1,m,n}+(\ )_{l+1,m,n-1} + (\ )_{l,m,n+1}-2(\ )_{l,m,n}+(\ )_{l,m,n-1}]. \tag{9d}$$

3.3. *Dependence zone*

For steady three-dimensional boundary layers, the calculation was found to have to follow the zone of dependence rule (Raetz 1957; Wang 1971). For steady, symmetry-plane problems, the wedge-shaped dependence zone shrinks to the symmetry-plane itself and it was found (Wang 1970) that the calculation stops at the onset of the reversal of the u-velocity profile, but the reversal of the v_θ-profile was unexpectedly calculated with no sign of any difficulty. This result was at first looked upon with suspicion, but later calculations of the full three-dimensional problems as well as the repeat calculations of the same symmetry-plane problem confirmed that the result was correct. However, a theoretical explanation was not available.

For unsteady cases in the two-dimensional or the symmetry-plane, an analogous zone of dependence (Wang 1975, 1979) must be observed. So at the beginning of the present work, the same question was raised again, i.e. what are precisely the differences in logic for the calculation of the u-profile and the v_θ-profile? In the unsteady case, we further know that the reversal of the u-profile can be calculated up to separation unlike in the steady case, where the calculation of the reversal of the u-profile is prohibited.

To provide the missing explanation, we carried out a characteristics study of the system of equations (1*a–c*). The determinants (Wang 1971) of the characteristics and subcharacteristics were found respectively to be

$$Q = -\nu^2\left(\frac{\partial\Omega}{\partial z}\right)^5, \tag{10a}$$

$$Q = \frac{\partial\Omega}{\partial z}\left(\frac{\partial\Omega}{\partial t}+\frac{u}{h_\mu}\frac{\partial\Omega}{\partial\mu}+w\frac{\partial\Omega}{\partial z}\right)^2, \tag{10b}$$

which shows that the addition of (1*b*) for v_θ (compared to equations for two-dimensional cases) merely increases the power (Wang 1975) from 3 to 5 in (10*a*) and from 1 to 2 in (10*b*). Otherwise, the same dependence rule applies to both the two-dimensional and the symmetry-plane problems. The underlying reason why the reversal of v_θ is not prohibited by the dependence rule is recognized due to the fact that in both (1*a*) and (1*b*), the differential operator

$$\frac{\partial}{\partial t}+u\frac{\partial}{h_\mu \partial \mu}+w\frac{\partial}{\partial z}$$

does not involve v_θ. Yet it it this operator which determines the subcharacteristics in (10*b*).

3.4. *Remarks about independence*

Historically there was some doubt about whether the symmetry-plane boundary layer could be determined independently of the adjacent boundary layer area. On initial inspection, this seems to violate the principle of upstream influence for a problem known to be initial-valued. This dilemma was difficult to solve precisely. Later, the concept of the zone of dependence did provide theoretical justification (Wang 1971) to this symmetry-plane approach. However, there still remain other puzzling questions.

For example, the symmetry-plane problem has often been interpreted to vaguely imply the following:

(i) The symmetry-plane boundary layer is independent of the rest of the boundary layer. It neither depends on the rest of the flow, nor does it influence the rest of the flow, and:

(ii) No fluid particle that does not lie in the symmetry-plane originally will ever reach that plane.

In the authors' view, these statements are not correct. The confusion seems to arise from the lack of distinction between the word 'independence' in the mathematical sense and in the physical sense. It is true that mathematically the symmetry-plane boundary-layer equations (1*a–c*) can be decoupled and solved separately from the rest, but it is confusing to state that the symmetry-plane flow is physically independent of the rest, because it is not. Equations (1*a*, *c*) differ from those for axisymmetrical boundary layers only in the presence of the term v_θ/r in (1*c*). This term, being a lateral derivative, oviously depends on the flow off the symmetry plane. Hence, physically the windside symmetry-plane flow does affect the rest of the flow, whereas the leeside symmetry-plane flow is affected by the rest of the flow.

Secondly, the fluid particles do leave (windside) and join (leeside) the symmetry plane. This can also be seen from the term v_θ/r in the continuity equation (1*c*). This term may be interpreted to represent the rate of mass addition (if $v_\theta < 0$). Confusion is usually caused by the argument: the cross-velocity v is identically equal to zero, so that the fluid particles cannot leave or join the symmetry-plane if they do not originally lie in the plane. This argument is actually not correct. Considering the leeside case, the fluid particles may be thought to approch the symmetry-plane symmetrically from two opposing sides; their cross-velocity v decreases as they move closer to the plane and become zero only when they reach the plane. Hence, the fluid can join the leeside symmetry-plane. Similarly, one can argue that the fluid can leave the windside symmetry-plane.

3.5. *Computational details*

The initial time t_0 was set to be 0.005 and the initial station μ_0 was taken at $\mu_s \pm 0.005$ where μ_s is the front stagnation point. With spatial initial profiles at μ_0, the calculation marches downstream at a fixed time t in an explicit fashion. At each μ-station, the solution between the body ($z = 0$) and the outer edge ($z \to \infty$) is calculated implicitly. The same process is repeated as time increases from t to $t + \Delta t$ until the results approach their steady-state values.

As the boundary layer grows, the number of steps in the z-direction must be increased; when that number exceeds 90, Δz is doubled.

Uneven steps were used in the μ-direction. Smaller $\Delta\mu$ were needed near both ends of the body where values of h_μ are relatively large and pressure gradients are strongly adverse. At first (Wang & Fan 1982) $\Delta t = 0.005$ were set for the case of 45° incidence. The skin friction was found to be oscillating as time passed 0.2; such oscillations were only removed after smaller $\Delta\mu$ and Δt were used. Large Δt can be used at large times. All different steps used in this work are listed in the report by Xu & Wang (1987). Δt varies from 0.001 to 0.005, $\Delta\mu$ from 0.000325 to 0.0025.

3.6. *Determination of unsteady separation*

The method of determining two-dimensional unsteady separation was once disputed, however it was later clarified (Van Dommelen & Shen 1980; Wang 1982; Zhang 1983). Van Dommelen & Shen identified separation by singularities in their Lagrangian type of calculation; Wang (1979) proposed to determine the separation by the convergence of analogous limiting streamlines in the (x, t)-plane. The latter idea was carried over from three-dimensional steady cases for which separation is determined by the convergence of limiting streamlines. For an impulsive-started circular cylinder, Wang's (1979) prediction of separation by this proposed criterion was in agreement with others (Van Dommelen & Shen 1980; Cowley 1983). The same criterion is applied to the present symmetry-plane problem to further test its validity; the results again agree with the steady-state values at large times.

4. Results

Calculations were made for a prolate spheroid of $b/a = 1/4$ at $\alpha = 6°$, 30°, 45° and 50°. Only the results of $\alpha = 6°$ and 30° will be presented here in order to exhibit the contrasting features between low and high incidence and between the windside and the leeside. The results of 45° and 50° follow the same pattern of 30°, only the skin friction $c_{f\mu}$ will be shown here because of its connection with discussions about separation.

For an impulsively started motion, pressure does not change with time, i.e. the same pressure as in the steady flow. The pressure variation along the symmetry-plane is shown in figure 2 (a, b). At higher incidence, the pressure gradients are larger. Larger pressure gradients appear to affect, among others, the rate of approach from unsteady conditions towards the final steady state. In the present calculations, the case of 50° incidence reaches the steady-state condition much faster than the case of 6° incidence.

4.1. $\alpha = 6°$, *leeside*

Figure 3 shows the variation of the skin friction $c_{f\mu}$. At a fixed μ-station, $c_{f\mu}$ decreases with time and steadily approaches its steady-state value. Such a decrease of $c_{f\mu}$ is expected from the fact that initially the boundary-layer thickness is nearly zero, so

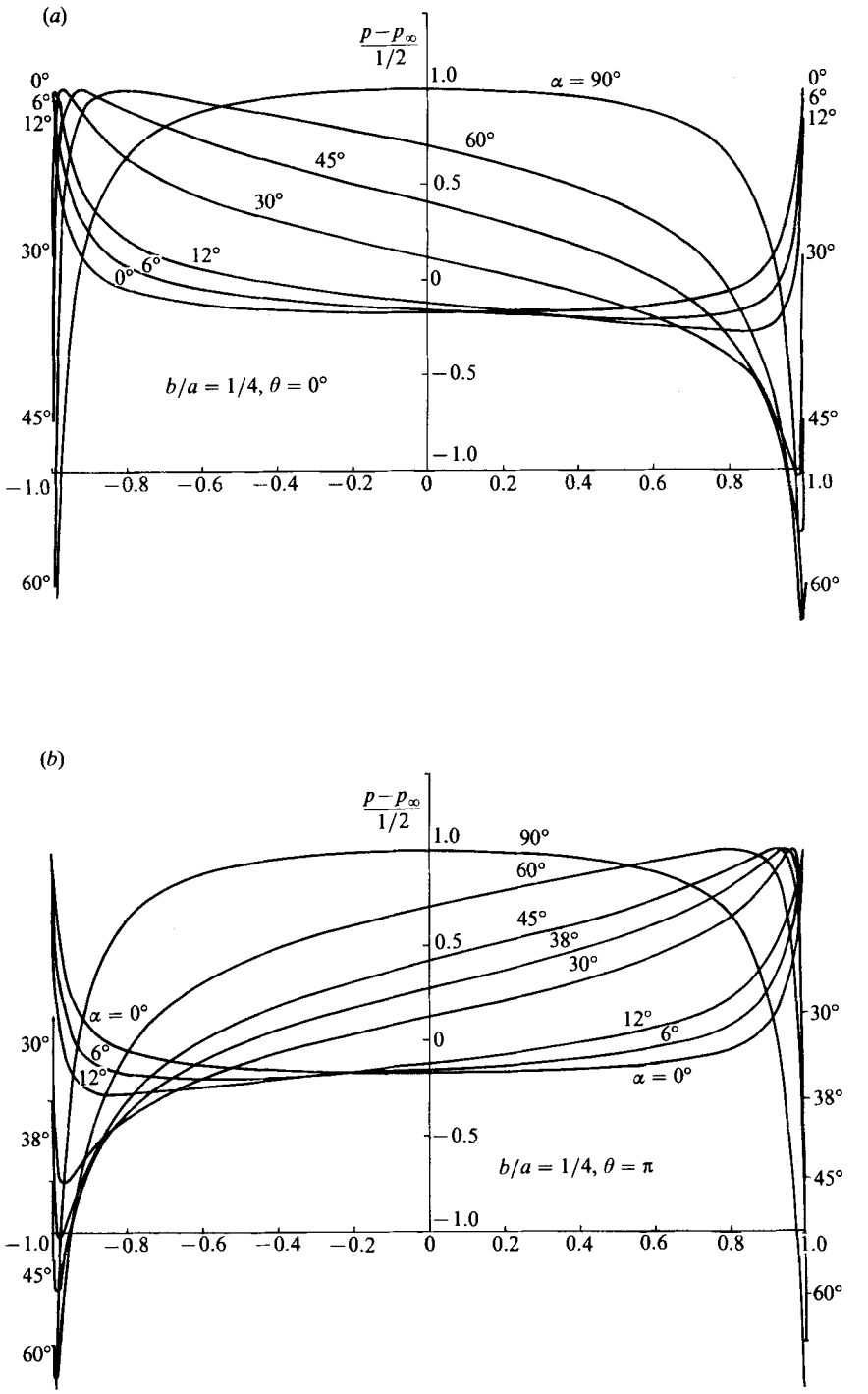

FIGURE 2. Pressure along the symmetry-plane. (*a*) Windside. (*b*) Leeside.

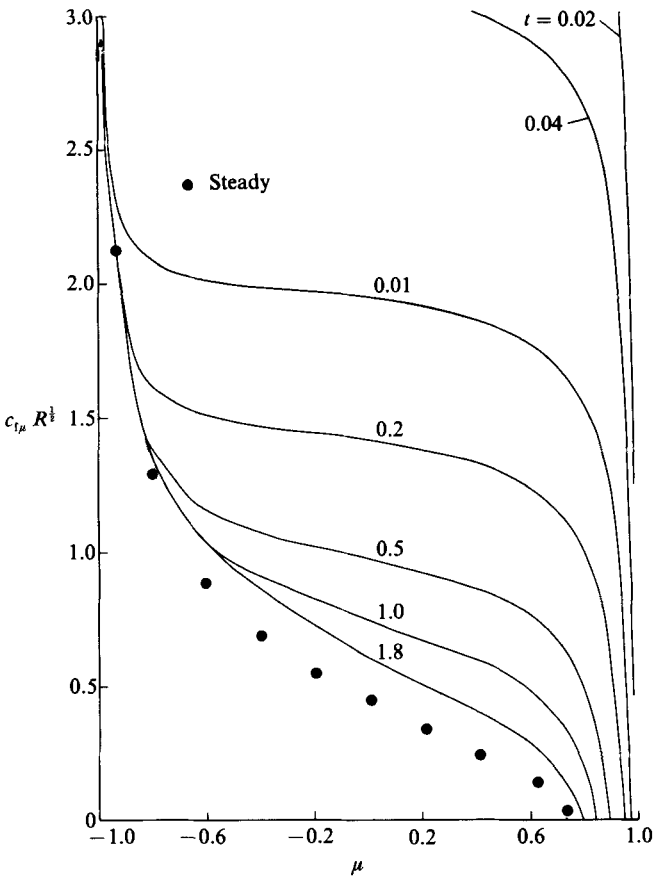

FIGURE 3. Leeside skin friction, $c_{f\mu}$ ($\alpha = 6°$).

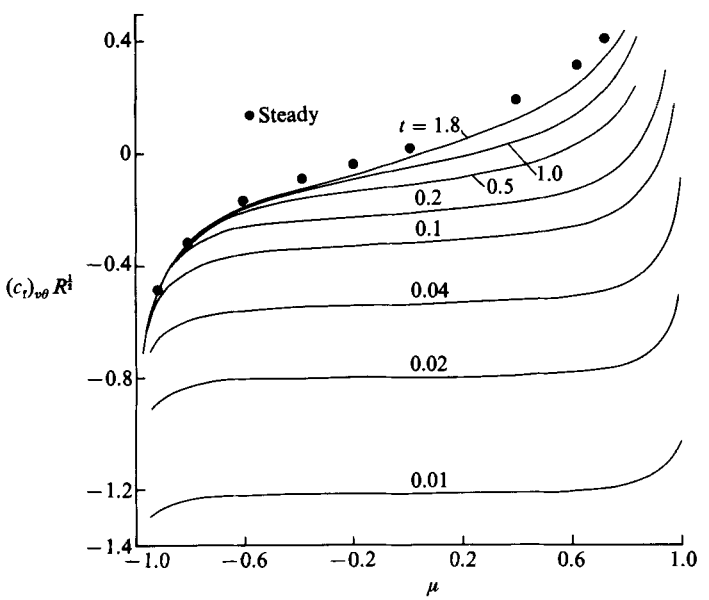

FIGURE 4. Leeside skin friction, $(c_f)_{v\theta}$ ($\alpha = 6°$).

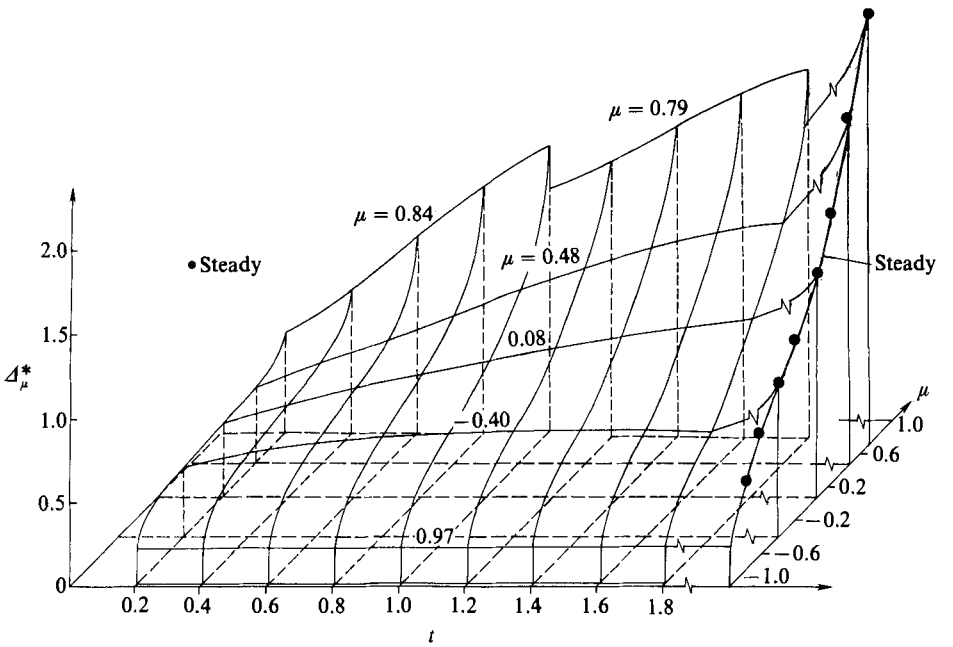

FIGURE 5. Leeside displacement thickness, Δ^*_μ ($\alpha = 6°$).

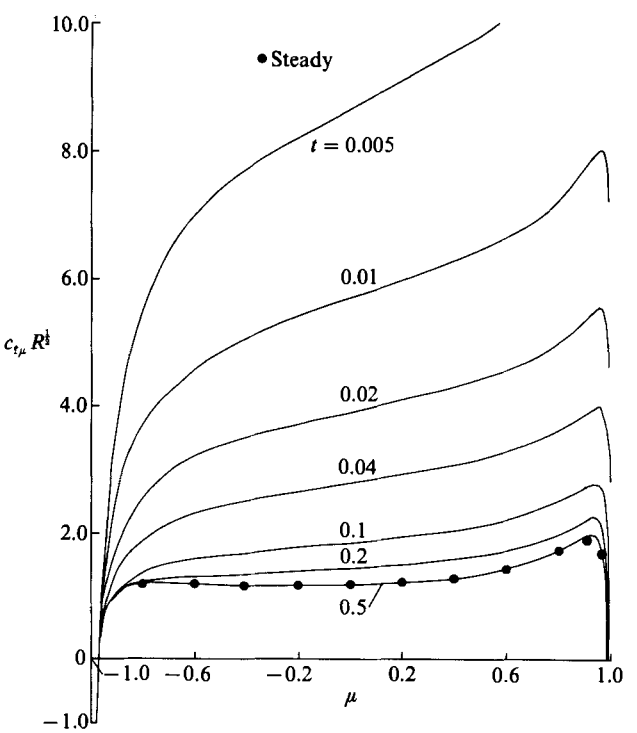

FIGURE 6. Windside skin friction, $c_{t\mu}$ ($\alpha = 30°$).

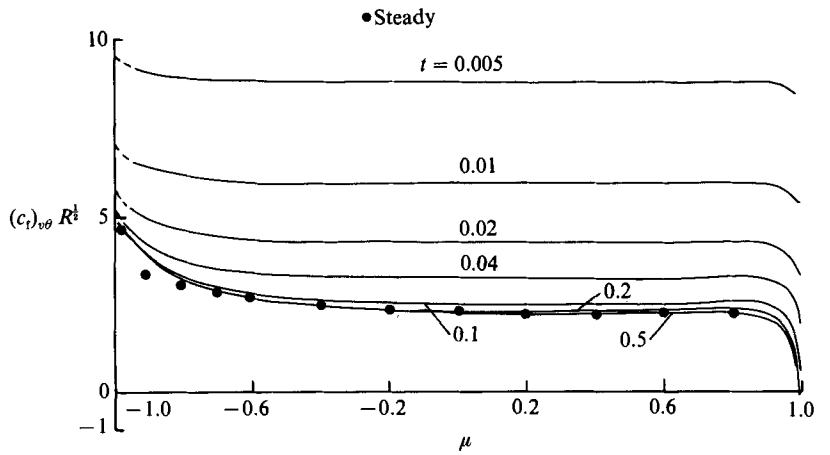

FIGURE 7. Windside skin friction, $(c_f)_{v\theta}$ ($\alpha = 30°$).

the skin friction is almost infinite. As time increases, the rate of approaching the steady state for the present low-incidence case becomes rather slow. At $t = 1.8$, which is a relatively large time compared to those for other cases calculated, the flow has not yet reached the steady state. At any fixed time, $c_{f\mu}$ first reaches a maximum near the vertex and then decreases rapidly in the nose region; along the rest of the symmetry-plane, $c_{f\mu}$ decreases rather gradually until near the rear end, when it drops to zero. The point where $c_{f\mu}$ vanishes is referred to as the zero-$c_{f\mu}$ point. In the present low-incidence case, the zero-$c_{f\mu}$ point gradually moves upstream as time increases. This is what is usually expected.

Figure 4 shows the variation of the analogous skin friction $(c_f)_{v\theta}$ based on the v_θ profiles. A change of sign of $(c_f)_{v\theta}$ signifies a reversal of v_θ-profiles; but near the symmetry-plane $v = (\partial v/\partial\theta)\,\Delta\theta$, hence reversal of the v_θ-profile implies reversal of the v-velocity near the symmetry-plane. At small times, $(c_f)_{v\theta}$ remains always negative, so there is no reversal of the v-velocity. As time increases, reversal of the v_θ-profile first occurs near the rear end and then gradually moves upstream. The point where $(c_f)_{v\theta}$ vanishes is referred to as the zero-$(c_f)_{v\theta}$ point. It is a characteristic of the present low-incidence case that both points of zero-$c_{f\mu}$ and of zero-$(c_f)_{v\theta}$ continue moving upstream with time. The importance of this behaviour is related to flow separation and will be discussed later.

Figure 5 shows the variation of the displacement thickness Δ^*_μ. As expected, Δ^*_μ increases with time at a fixed μ-station and increases from the front towards the rear along the body at any fixed time.

4.2. $\alpha = 30°$, *windside and leeside*

High-incidence flow displays more unconventional features. Both windside and leeside were calculated, and these results are presented here to show typical differences between the windside and the leeside. The leeside results are further compared with the same for $\alpha = 6°$ to exhibit the incidence effects.

Figures 6–8 give the windside skin frictions $c_{f\mu}$, $(c_f)_{v\theta}$ and displacement thickness Δ^*_μ. $c_{f\mu}$ increases all the time along the body, except near the rear end, but decreases at a fixed-station as time increases. The steady-state condition of $c_{f\mu}$ was reached at $t = 0.5$. $(c_f)_{v\theta}$ is positive on the windside and remains always nearly constant along

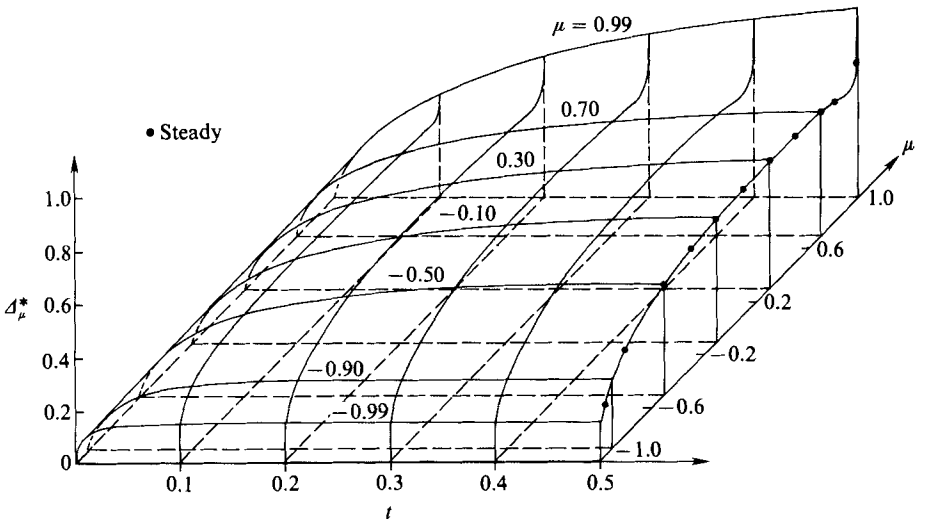

FIGURE 8. Windside displacement thickness, Δ_μ^* ($\alpha = 30°$).

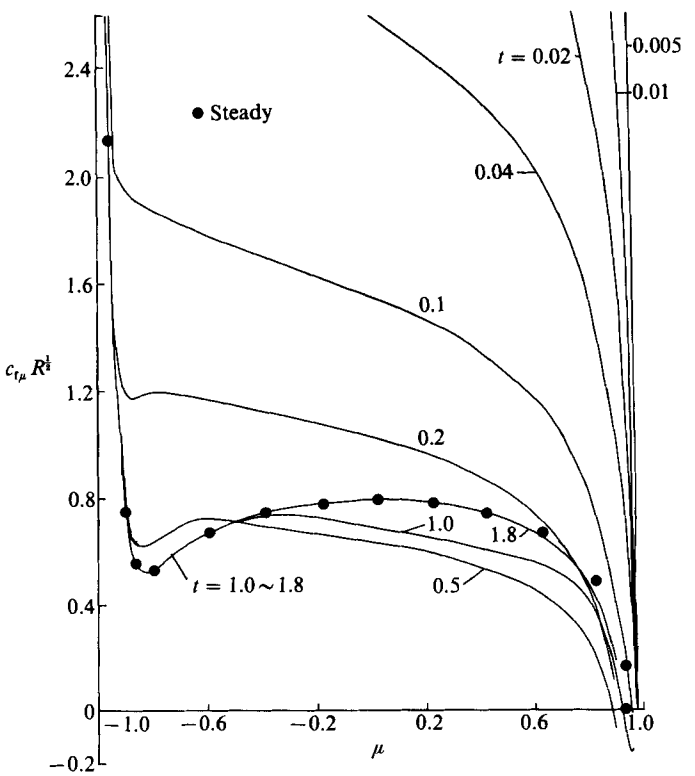

FIGURE 9. Leeside skin friction, $c_{f\mu}$ ($\alpha = 30°$).

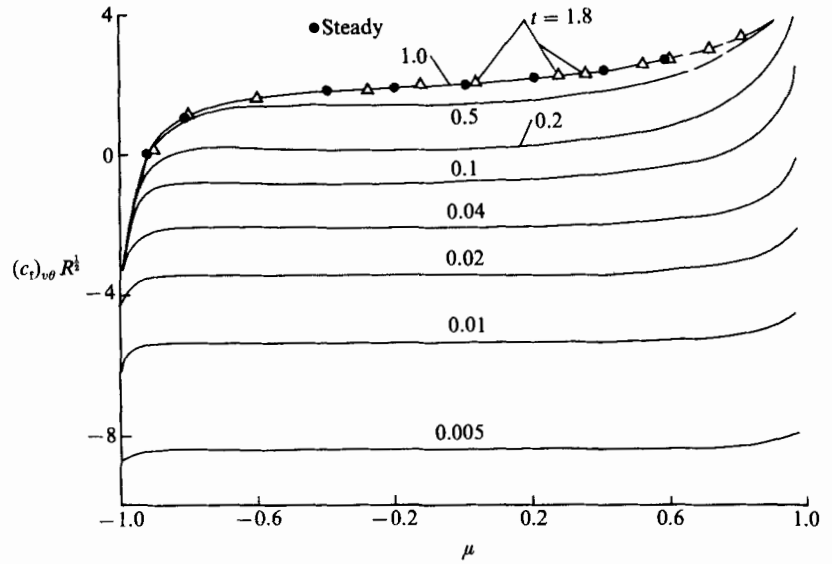

FIGURE 10. Leeside skin friction, $(c_f)_{v\theta}$ ($\alpha = 30°$).

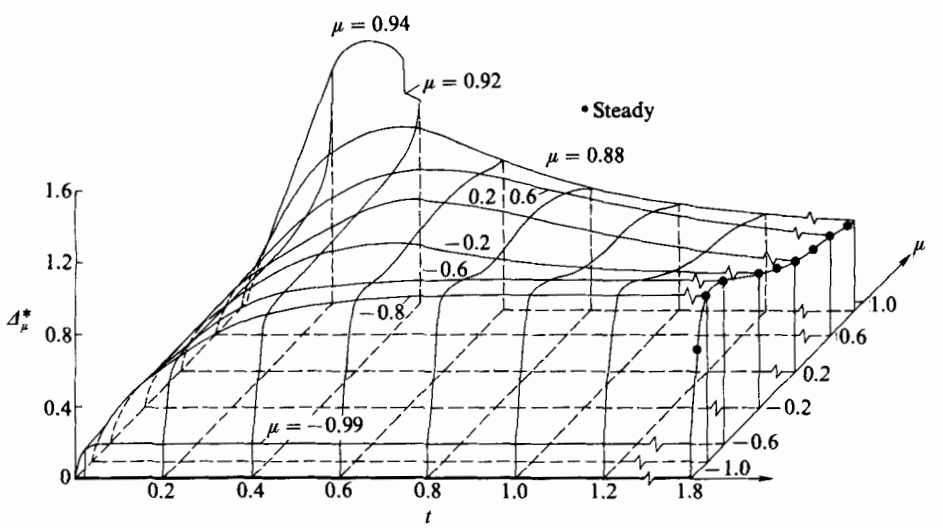

FIGURE 11. Leeside displacement thickness, Δ_μ^* ($\alpha = 30°$).

the body except near two ends. This implies that at such a high incidence, $(c_f)_{v\theta}$ never becomes zero (or the v-velocity profile never reverses near the body) on the windside except at the very rear end. The situation is different in the case of 6° incidence although the relevant result is not included here. Δ_μ^* increases as expected along the body at any fixed time and at a fixed point as time changes. Good agreement with its steady-state value is again seen at $t = 0.5$.

Leeside calculations generally require a longer time to reach the steady-state conditions. At small times, the skin friction $c_{f\mu}$ (figure 9) varies just like that of the 6° incidence case (figure 3), i.e. it decreases with increasing time at a fixed μ-station and along the body at a fixed time; the point of zero-$c_{f\mu}$ moves upstream only very little. At large times, these trends, however, no longer hold. There appears then a

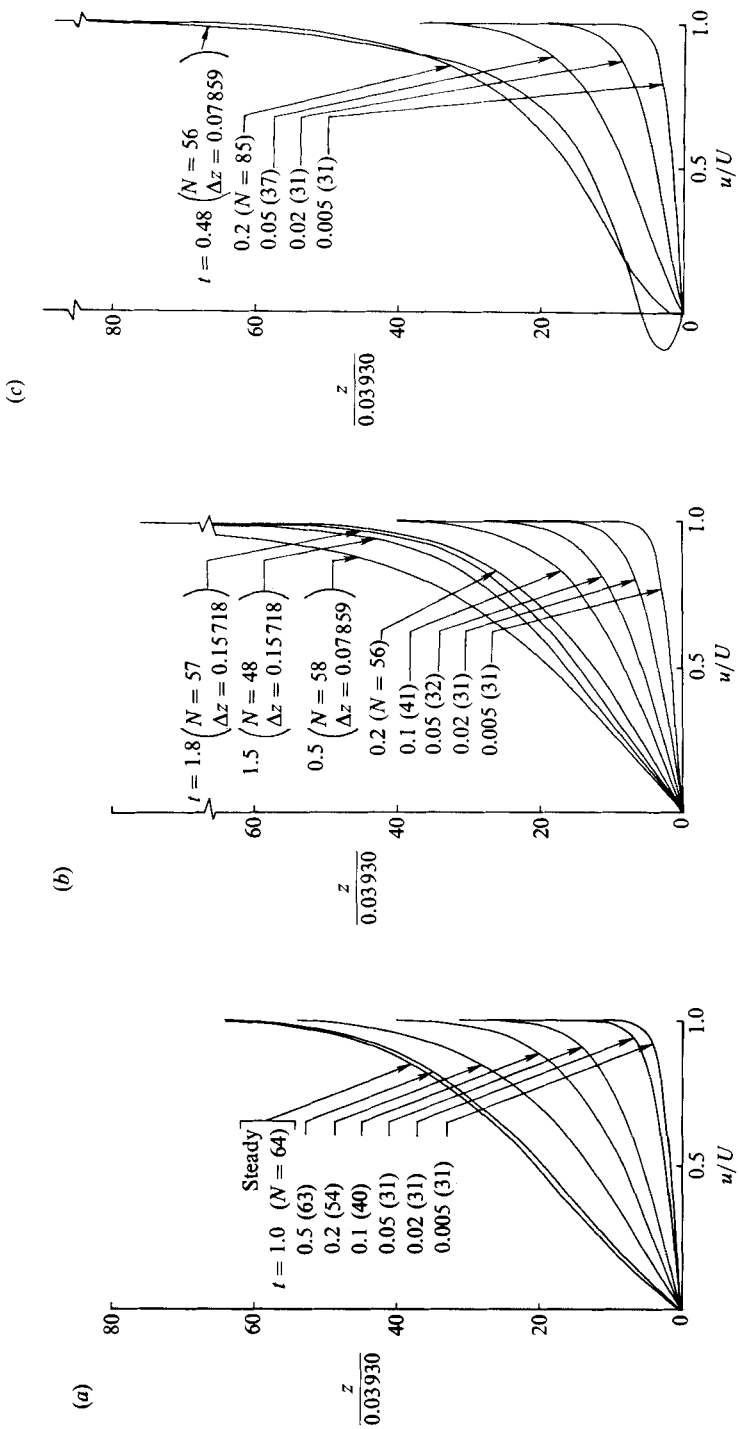

FIGURE 12. u-velocity profile, leeside, $\alpha = 30°$: $N = z_{max}/\Delta z$; $\Delta z = 0.0393$ (unless specified). (*a*) $\mu = -0.841$. (*b*) $\mu = 0.038$. (*c*) $\mu = 0.958$.

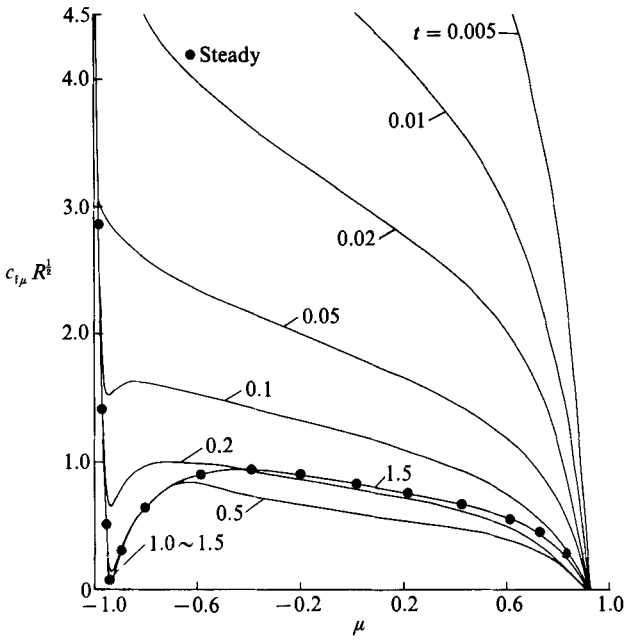

FIGURE 13. Leeside skin friction, c_{f_μ} ($\alpha = 45°$).

minimum point in the c_{f_μ} curves in the nose region beginning at about $t = 0.46$. This minimum continues to dip until a steady-state value (0.51) is reached at approximately $t = 1.0$. After passing the minimum point, c_{f_μ} increases over the most part of the rest of the body before dropping to zero over the aft body. Steady-state condition was approached at approximately $t = 1.8$, the zero-c_{f_μ} point does not only not move upstream, but also tends to shift slightly downstream. The overall change, however, is so small that the zero-c_{f_μ} point may be considered to stay always near the rear stagnation point. The unconventional behaviour of c_{f_μ} described here leads to different unsteady separation patterns at different incidence; this will be discussed in §5.

The $(c_f)_{v\theta}$ for 30° incidence (figure 10) shows similar trends as that for 6° incidence except that the steady-state condition was reached much sooner. An important difference is that the zero-$(c_f)_{v\theta}$ point shifts from the rear to the nose so fast as to be in a jump manner. As seen in figure 10, this point is located at the rear at $t = 0.10$, but moves to the nose at $t = 0.2$.

At small times ($t < 0.3$), the displacement thickness, Δ^*_μ (figure 11), increases from the nose to the rear, the same as in the 6° incidence case. However, this trend is changed for $t > 0.3$. Then, after a rapid increase near the nose, Δ^*_μ gradually decreases over the rest of the body. Note that the curves for $\mu > 0.90$ are shown only up to $t = 0.5$; this is because, as the zero-c_{f_μ} point moves upstream, calculation cannot be continued much further.

The reasons why c_{f_μ} and Δ^*_μ for 30° incidence behave differently in comparison with those for 6° incidence can all be found from the results of the u-velocity profiles. At a front station ($v = -0.8411$, figure 12*a*), the profiles continue to steepen at all times. This is consistent with the usual boundary-layer trend, which holds also for the 6° incidence. But this trend is no longer followed along the rest of the body at 30°

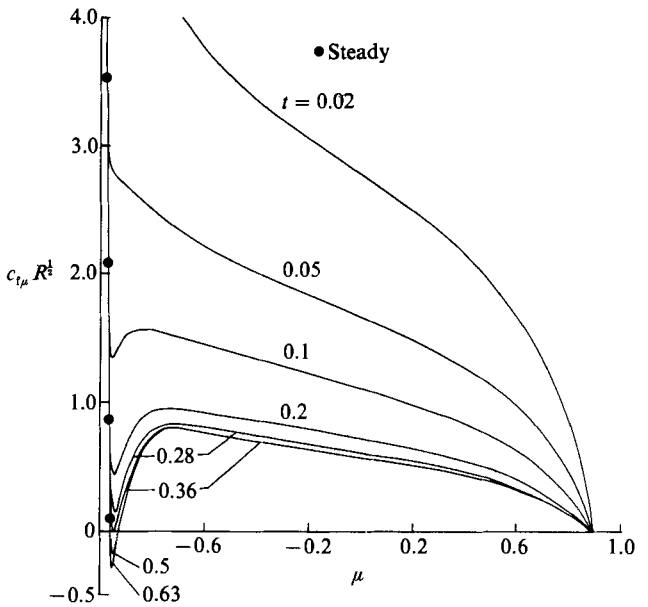

FIGURE 14. Leeside skin friction, $c_{f\mu}$ ($\alpha = 50°$).

incidence. At a mid-station ($\mu = 0.038$, figure 12*b*), the profiles first steepen up at small times, but flatten down at large times. Similarly, at a rear station ($\mu = 0.9588$, figure 12*c*), the profiles cross each other at large times.

4.3. $\alpha = 45°$, *and* $50°$

The results for $\alpha = 45°$ and $50°$ are generally similar to those for $\alpha = 30°$, only the effects of increasing incidence discussed in §4.2 become more pronounced and the approach to steady-state is faster.

For $\alpha = 45°$, the leeside skin friction $c_{f\mu}$ (figure 13) forms a minimum near the nose at a much earlier time ($t = 0.10$) and this minimum continues to dip until approaching its steady-state value of 0.034 at $\mu = -0.933$ and $t = 1.5$. Thus $c_{f\mu}$ still does not become zero over the forebody. The same conclusion was reported by Wang & Fan (1982). Similar to the $\alpha = 30°$ case, the zero-$c_{f\mu}$ point stays near the rear stagnation point almost unchanged for all the times.

For $\alpha = 50°$, a distinct feature is, however, noted in the variation of $c_{f\mu}$ (figure 14). While the zero-$c_{f\mu}$ point at early times remains at the rear stagnation point, the $c_{f\mu}$-minimum over the forebody appears earlier and quickly dips to zero at $t = 0.35$ and $\mu = -0.946$. When this happens, the zero-$c_{f\mu}$ point jumps from the aftbody to the forebody. At $t = 0.60$, $c_{f\mu}$ becomes zero at $\mu = -0.9547$ and -0.9272, its minimum value is -0.2421 at $\mu = -0.9538$. After $t = 0.63$, when the minimum becomes -0.2811, the calculation was terminated at $\mu = -0.967$ because the steep increase of the displacement thickness signified separation.

Based on (6), analogous limiting streamlines are drawn in the (μ, t)-plane (figure 15) for $\alpha = 50°$. The arrows indicate the slope at each coordinate point. The lines drawn tangent to these arrows are the limiting streamlines analogous to steady three-dimensional cases. The convergence of these lines signifies unsteady separation. Figure 15 indicates that separation starts around $t = 0.63$ at $\mu = -0.957$ and

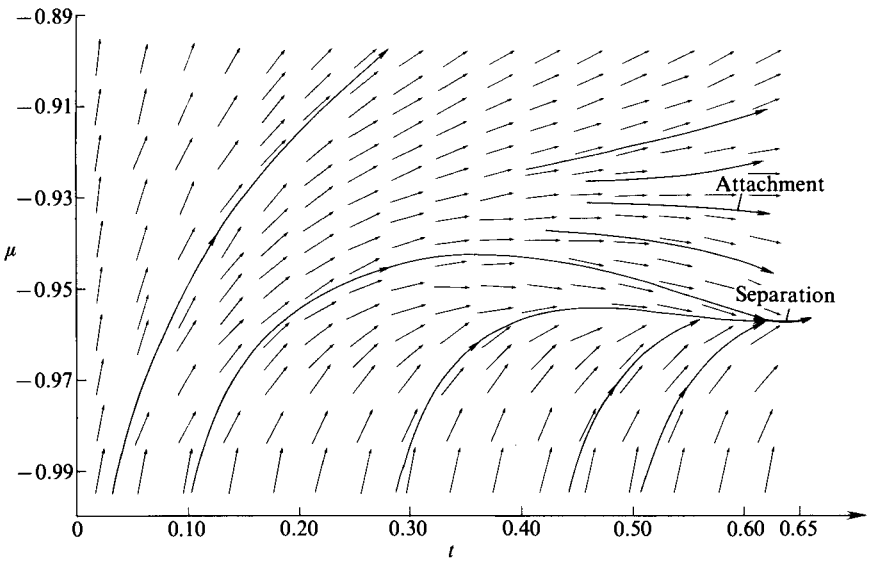

FIGURE 15. Unsteady limiting flow pattern and separation line in the (μ, t)-plane. Leeside, $\alpha = 50°$.

correctly approaches its steady-state value at large times. Similarly the line from which limiting streamlines diverge is the analogous line of unsteady attachment.

5. Discussions

From the preceding solutions on the windside and leeside symmetry-plane, especially the pattern of variation of $c_{f\mu}$ and $(c_f)_{v\theta}$, we shall now attempt to suggest a possible unsteady separation sequence over the whole body. The same logic was used previously by Wang (1972) for the steady case, and the predicted sequence was later confirmed by experiments and full three-dimensional calculations over the whole body.

Wang & Fan (1982) reported that there is a similarity in the skin friction pattern of the leeside symmetry-plane between the previous steady case with incidence α as the varying parameter and the present unsteady cases with time as the parameter. Our current more comprehensive calculations provide further evidence in support of this similarity. Reproduced in figure 16 is the steady leeside $c_{f\mu}$ varying with incidence. Comparing figure 16 to figures 9, 13 and 14 for the unsteady $c_{f\mu}$, the similarity is apparent. In these figures, there appears a minimum point in the $c_{f\mu}$-curve near the nose when incidence is large enough in the steady case or time is large enough in the unsteady case. This minimum dips further and eventually becomes zero at high incidence and large times.

For the steady symmetry-plane problem, the point of vanishing $c_{f\mu}$ is also the point of separation. For the unsteady case, although the vanishing of $c_{f\mu}$ is not synonymous with separation, unsteady separation occurs only after $c_{f\mu}$ becomes zero first and then negative. In other words, the vanishing of $c_{f\mu}$ is a precondition of unsteady separation.

Mainly on the basis of figure 16, it was argued (Wang 1972) that steady separation patterns over the whole body follow a closed–open–closed cycle, i.e. closed at low

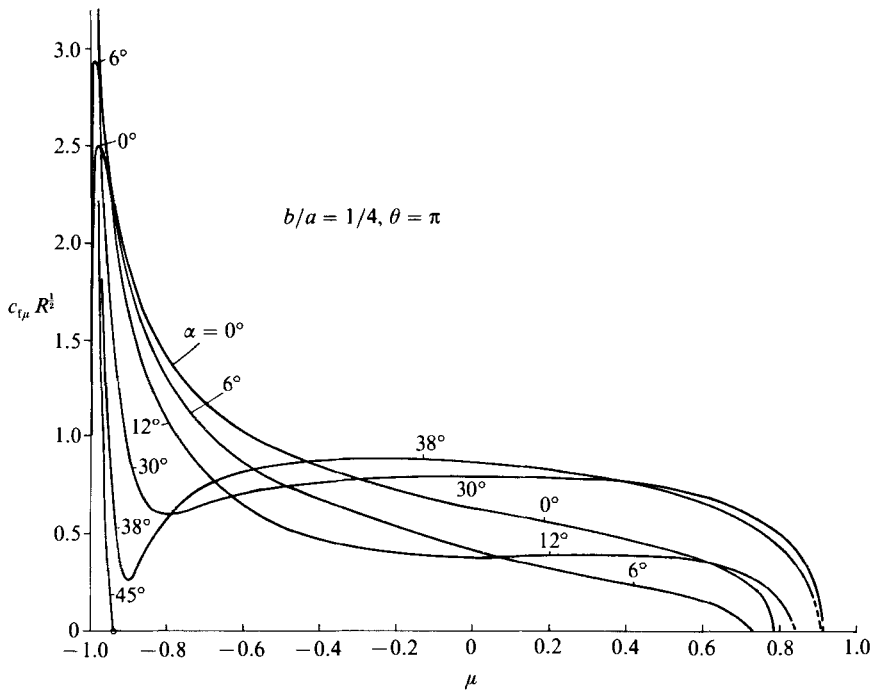

FIGURE 16. Leeside steady skin friction, $c_{f\mu}$.

incidence (6°), open at moderate incidence (30°) and closed again at extremely high incidence for a prolate spheroid of axis-ratio 1/4 (figure 17). Based on the aforenoted similarity, we shall now attempt to depict analogously an unsteady separation sequence.

5.1. $\alpha = 6°$, *low incidence*

Figures 3–4 show that both the zero-$c_{f\mu}$ point, S, and the zero-$(c_f)_{v\theta}$ point, R, start at the rear stagnation point and then continue moving upstream as time increases. R moves faster and is always located ahead of S. The corresponding flow pattern near the symmetry-plane is illustrated in figure 18(a). Also superimposed in figure 18(a) is the steady-state separation line from previous steady calculations. The steady-state value for R on the leeside is $\mu = -0.084$. With so much information known on the symmetry-planes and the steady-state separation curve as a guide, it is argued that separation along all other meridians ($0° < \theta < 180°$) will vary similarly as along the symmetry-plane, so that the separation lines are confined on the aft-body and are closed curves as illustrated in figure 18(b). As time increases, the closed separation line gradually expands upstream.

5.2. $\alpha = 30, 45°$, *moderate incidence*

At $\alpha = 30°$, the zero-$c_{f\mu}$ point, S, along the leeside symmetry-plane ($\theta = 180°$) remains near the rear stagnation point, while the corresponding zero-$(c_f)_{v\theta}$ point, R, moves quickly to the front nose (figure 10) and its steady-state location is at $\mu = -0.910$. The minimum value of $c_{f\mu}$ near the nose never becomes zero. This implies that separation on the leeside symmetry-plane is kept at the rear end all the time.

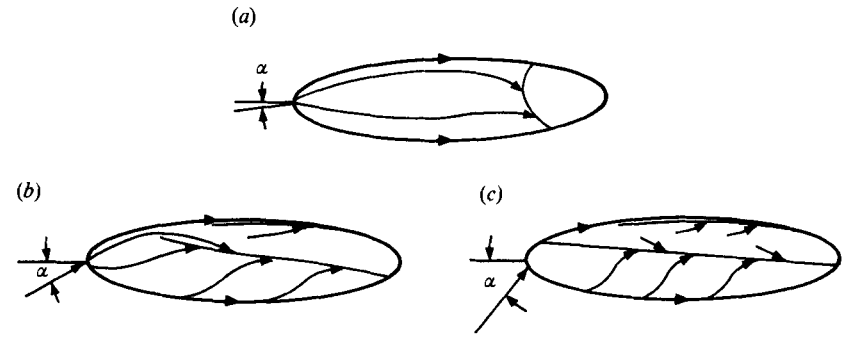

FIGURE 17. Steady separation sequence. (*a*) Low α. (*b*) High α. (*c*) Extremely high α.

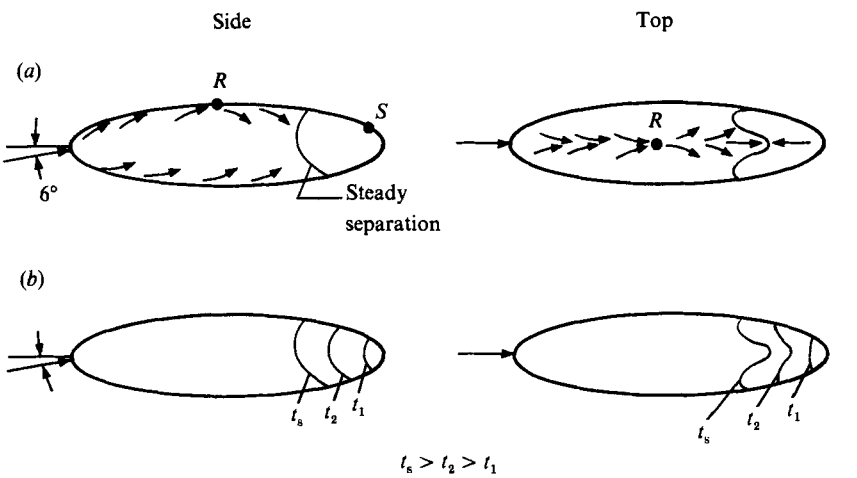

FIGURE 18. Separation at low incidence (6°). (*a*) Flow near the symmetry-plane and steady separation line. (*b*) Unsteady separation sequence.

The windside (i.e. $\theta = 0°$) R and S always remain at the very rear end. The flow pattern near the symmetry-planes are illustrated in figure 19(*a*), where the primary and secondary open-separation lines for the steady case are also superimposed. Based on this information, it is argued that while the separation point on the leeside symmetry-plane remains always near the rear stagnation point, the separation points along other meridians ($0 < \theta < 180°$) off the symmetry plane must move upstream. This is because, at such relatively high incidence, the circumferential flow over most of the body is subject to a larger adverse pressure gradient than the meridional flow; a mainly cross-flow separation must occur on two sides of the symmetry-plane at much earlier times. The resulting separation line on the whole body is expected to be of the closed type at small times (figure 19*b*), and gradually expands upstream as depicted in figure 19(*c*). This latter pattern cannot continue too long; it must break open (figure 19*d*) in order to match its steady-state condition (figure 19*e*).

The state of affairs for $\alpha = 45°$ is similar to what was just described for $\alpha = 30°$, except the steady-state primary separation line is almost closed, even though theoretically it is still open, because $c_{t\mu}$ did not become exactly zero at large times. The same result was found by Wang & Fan (1982). At that time, steady separation

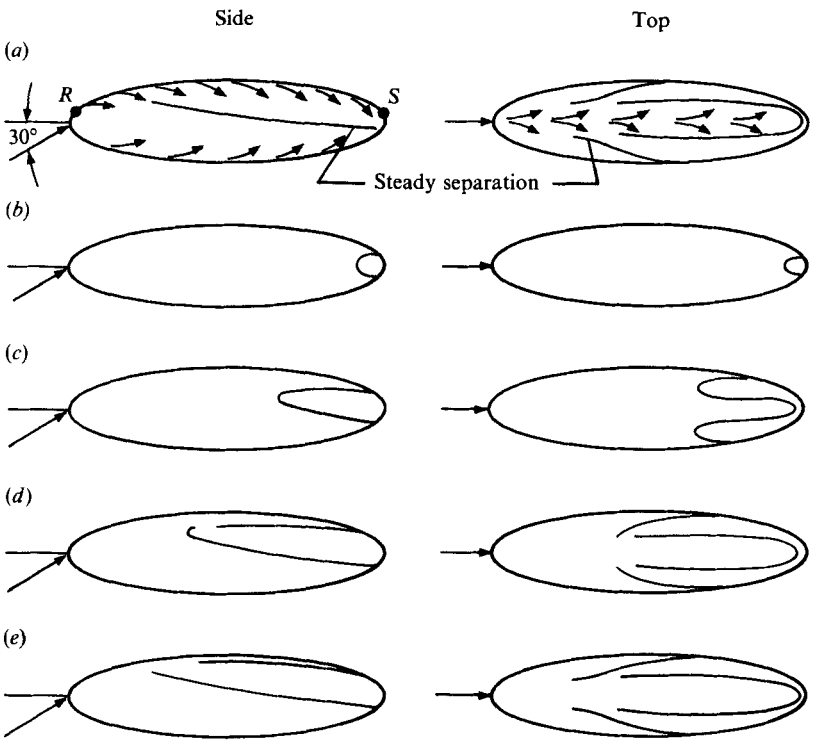

FIGURE 19. Separation at moderate incidence (30°). (a) Flow near the symmetry-plane and steady separation line. (b)–(e) Unsteady separation sequence; (b) small time, t_1, (c) $t_2 > t_1$, (d) $t_3 > t_2$, starting of open separation, (e) large time.

according to earlier calculations was known to be closed, i.e. $c_{f\mu}$ does go to zero, over the forebody at 45° incidence. This led to the interpretation that the unsteady approach towards the steady-state condition can only be achieved asymptotically as time becomes infinite. In the present work, steady solutions for $\alpha = 45°$ were recalculated with different step sizes, $h_\mu \Delta\mu = 0.004$, 0.003, 0.002, 0.0015 and 0.001. It was found that whether $c_{f\mu}$ in the forebody goes to zero or not depends on the step size used. For $h_\mu \Delta\mu$ greater than 0.0015, $c_{f\mu}$ did become zero over the forebody, but for $h_\mu \Delta\mu$ equal to or smaller than 0.0015, c_f did not reach zero, though it was very close. Thus, these repeated calculations make the steady and unsteady results consistent with each other.

5.3. $\alpha = 50°$, *high incidence*

The main difference between $\alpha = 50°$ and the preceding cases of $\alpha = 30°$ and 45° is that the minimum $c_{f\mu}$ near the nose finally becomes zero and even negative. The unsteady separation pattern is expected to go through the same sequence (figures 19*b–d*) except that the primary separation line becomes closed as the steady-state condition is approached (figure 20*a*).

Between $0.35 < t < 0.63$, $c_{f\mu}$ near the nose changes from positive to negative and then back from negative to positive. This implies a short recirculating bubble (figure 20*a*) imbursed inside the boundary layer. This bubble is likely to become longer (figure 20*b*) as the incidence increases to 60° or 70°. At still higher incidence, a second

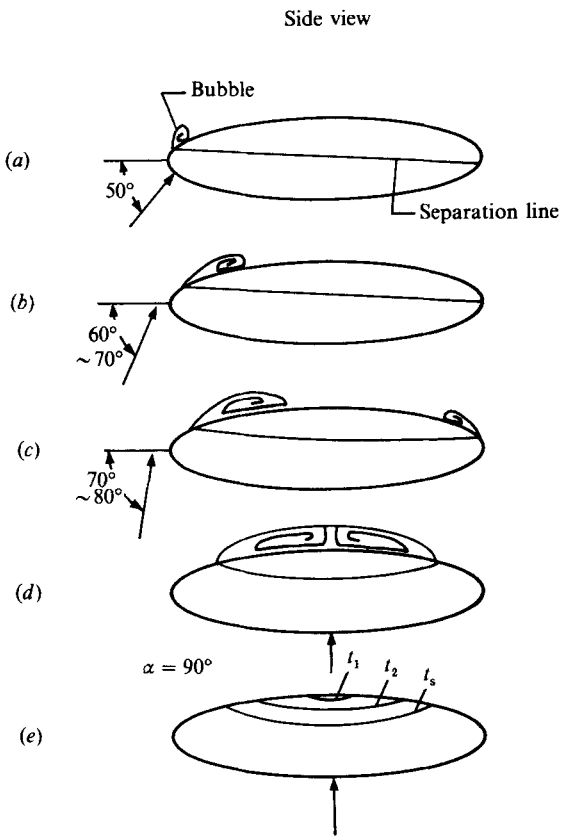

FIGURE 20. (*a*)–(*d*) Separation line and separation bubble at large times. (*e*) Unsteady separation sequence at $\alpha = 90°$.

bubble emerges on the aft body (figure 20*c*). In the limiting case of 90° incidence, the separation pattern becomes symmetrical with the mid-section (figure 20*d*). The unsteady sequence for $\alpha = 90°$ is expected to consist of a series of closed separation lines (figure 20*e*).

5.4. *Less slender bodies*

The preceding proposed unsteady separation sequence is based on the results for a prolate spheroid of $b/a = 1/4$. It is expected that the same will apply to more slender shapes such as $b/a = 1/6$, but not for less slender cases such as $b/a = 1/2$. As the ratio b/a increases, a prolate spheroid becomes more like a sphere so there will then be no open separation involved and the unsteady separation sequence will consist of a series of closed separation lines only.

For bodies other than a spheroid, a similar unsteady sequence may be conceived. For example, in the case of an impulsively-started blunt cone, open separation lines start at small times over the rear body and gradually extend forward as time increases. Depending upon the cone angle, nose radius and incidence, the steady-state separation at large times may remain either open or closed.

6. Conclusions

The unsteady laminar boundary layers along the symmetry-plane of an impulsively-started prolate spheroid of axes ratio of 1/4 are calculated here for incidence 6°, 30°, 45° and 50°. The large-time results agree very well with those obtained previously from steady-flow calculations.

A similarity was found in the skin friction pattern of the leeside symmetry-plane between the present unsteady case with time as the varying parameter. As time increases, the zero skin friction point at low incidence (6°) continues moving upstream from the rear stagnation point until it reaches its steady-state location. At moderate incidence (30°, 45°), it remains always near the rear stagnation point. At still higher incidence (50°), it does not move for a long time until it finally jumps to the front nose.

Based on the leeside skin friction patterns, it was argued in the steady case that separation follows a closed–open–closed cycle; i.e. over a prolate spheroid of 1/4, a closed separation prevails at low incidence, open separation at moderate incidence and closed separation again at high incidence. This steady separation cycle has later been confirmed by experiment and more complete calculations of three-dimensional boundary layers.

Because of the above noted similarity in the leeside skin friction behaviour, analogous unsteady separation sequences are suggested. At low incidence (6°), the separation line starts around the rear stagnation point, and continues to extend upstream until it approaches the steady-state position. At all times, however, separation is of the closed type. At moderate to high incidence (30°, 45°, 50°), closed separation develops at small times, but open separation at large times. On approaching the steady-state condition, separation may either remain open ($\alpha = 30°$, 45°) or become closed ($\alpha = 50°$). Thus the open *vs.* closed separation sequence originally developed for steady flows appears to have found a counterpart in unsteady flows.

For a less slender spheroid such as $b/a = 1/2$, there is no open separation involved, unsteady separation lines are all of the closed type. Similar ideas hold for general bodies other than spheroids.

Note added in proof. Recent extensive experiments show that steady separation is closed at $\alpha \leqslant 5°$, but becomes marginally open at 6°. Hence, the discussion in §5.1 for large times applies more appropriately to $\alpha \leqslant 5°$ rather than $\alpha \leqslant 6°$. Details will be reported later.

REFERENCES

CEBECI, T., KHATTAB, A. K. & STEWARTSON, K. 1980 On nose separation. *J. Fluid Mech.* **97**, 435–454.

COWLEY, S. J. 1983 Computer extension and analytic continuation of Blasius' expansion for impulsive flow past a circular cylinder. *J. Fluid Mech.* **135**, 389–405.

KRAUSE, E. 1969 Comment on solution of a three-dimensional boundary-layer flow with separation. *AIAA J.* **7**, 575–576.

MOORE, F. K. & OSTRACH, S. 1957 Displacement thickness of the unsteady boundary layer. *J. Aero. Sci.* **24**, 77–78.

RAETZ, G. S. 1957 A method of calculating three-dimensional laminar boundary layers of steady compressible flows. *Rep. No. NAI* 58-73, Northrop Corporation, CA.

VAN DOMMELEN, L. L. & SHEN, S. F. 1980 The spontaneous generation of the singularity in a separating laminar boundary layer. *J. Comp. Phys.* **38**, 125–140.

VAN DOMMELEN, L. L. & SHEN, S. F. 1982 The genesis of separation. In *Numerical and Physical Aspects of Aerodynamics Flows* (ed. T. Cebeci), pp. 293–311. Springer.

WANG, K. C. 1970 Three-dimensional boundary layer near the plane of symmetry of a spheroid at incidence. *J. Fluid Mech.* **43**, 187–209.

WANG, K. C. 1971 On the determination of the zones of influence and dependence for three-dimensional boundary layer equation. *J. Fluid Mech.* **48**, 397–404.

WANG, K. C. 1972 Separation pattern of boundary layer over an inclined body of revolution. *AIAA J.* **10**, 1044–1050.

WANG, K. C. 1974 Boundary layer over a blunt body at high incidence with an open-type of separation. *Proc. R. Soc. Lond.* A **340**, 33–55.

WANG, K. C. 1975 Aspects of multi-time initial valued problem originating from boundary layer equations. *Phys. Fluids* **18**, 951–955.

WANG, K. C. 1979 Unsteady boundary layer separation. *Martin Marietta Labs Rep.* TR-79-16c.

WANG, K. C. 1982 On the disputes of unsteady separation. In *Numerical and Physical Aspects of Aerodynamic Flows* (ed. T. Cebeci), pp. 279–291. Springer.

WANG, K. C. & FAN, Z. G. 1982 Unsteady symmetry-plane boundary layer and 3-D unsteady separation. *AF&EM* TR-82-01, San Diego State University.

XU, W. & WANG, K. C. 1987 Unsteady laminar boundary layer along the symmetry-plane of an impulsively-started prolate spheroid. *AE&EM* TR-87-01, San Diego State University.

ZHANG, H. X. 1983 A general criterion for two-dimensional flow separation. *Acta Mech. Sin.* **6**, 559–570.